



Development and functionality analysis of lipoplex-loaded polysaccharide-based surface coatings for local nucleic acid delivery

Maria Krabbes ^a, Vincent Kampik ^a, Jan Krieghoff ^a, Vivian Haas ^b, Mathilde Heizmann ^b, Maria Morawietz ^c, Hermann Kalwa ^d, Leonard Kaysser ^b, Clara T. Schoeder ^b, Karsten Mäder ^e, Christian E.H. Schmelzer ^a, Michaela Schulz-Siegmund ^a, Christian Wölk ^a*

^a Institute of Pharmacy, Faculty of Medicine, Leipzig University, Leipzig, Saxony, Germany

^b Institute for Drug Discovery, Faculty of Medicine, Leipzig University, Leipzig, Saxony, Germany

^c Fraunhofer Institute for Microstructure of Materials and Systems IMWS, Halle (Saale), Saxony-Anhalt, Germany

^d Rudolf-Boehm-Institute for Pharmacology and Toxicology, Faculty of Medicine, Leipzig University, Leipzig, Saxony, Germany

^e Institute of Pharmacy, Faculty of Science I, MLU Halle-Wittenberg, Halle (Saale), Saxony-Anhalt, Germany

ARTICLE INFO

Keywords:

Local nucleic acid delivery

LbL

Lipid nanoparticles

Polyelectrolyte multilayers

ABSTRACT

Although therapeutic nucleic acids reached the clinical application for a decade, the success of these new drugs is dependent on their delivery strategies, which are still a challenge. In particular, local delivery of nucleic acids is a promising approach to develop therapies with a spatially controlled site of action. However, compared to techniques for systemic administration, local nucleic acid delivery systems are still rarely described. In this study, we present a promising approach to fill this gap by the design of surface coatings based on polysaccharides for local delivery of nucleic acids. An automatized Layer-by-Layer deposition approach was applied using hyaluronic acid and chitosan to form polyelectrolyte multilayer systems, into which lipid nanoparticles, more specific lipoplexes, were embedded as nucleic acid carriers. Different manufacturing parameters, in particular the number of deposited polyelectrolyte layers and the preparation buffer, were varied. The multilayer film characteristics were investigated systematically regarding their physical properties, with a focus on thickness and topology as well as lipoplex deposition, to identify a system with efficient transfection properties. The multilayer systems prepared in acetate buffer were characterized by a good lipoplex embedding with a more uniform distribution and lower tendency for formation of large lipoplex aggregates in the polyelectrolyte film. Additionally, we were able to demonstrate the functionality of the developed system for nucleic acid delivery. The nucleic acids were successfully transferred into cells in a contact-triggered manner. Furthermore, we could demonstrate the enzymatic degradation-based release of nucleic acid cargo from the delivery system caused by hyaluronidase, followed by successful *in vitro* transfection.

1. Introduction

Nucleic acids have great potential as therapeutics, enabling the exogenous regulation of cellular processes by permanent or transient changes in gene expression. This is referred to as gene therapy. Therefore, disease-related genes can be altered with therapeutic nucleic acids by adding, removing, or replacing genetic material as well as activating and suppressing gene expression (Piotrowski-Daspit et al., 2020).

The application of nucleic acids as functional drug molecules offers new treatment options to cure diseases on their molecular level, but also raises particular requirements in terms of administration and drug formulation. Specific difficulties for this class of active pharmaceutical ingredients include their rapid enzymatic degradation and the inability

to pass biomembranes due to their high molecular weight and high negative charge density (Lin and Qi, 2023). In order to guarantee an effective and safe therapy with nucleic acids, the right delivery systems are of central and decisive importance (Sung and Kim, 2019). The development of delivery strategies to overcome biological barriers and enable the intracellular uptake of nucleic acids has been extensively explored in recent years, but remains a major challenge for nucleic acids (Mendes et al., 2022).

Particularly, local application has the potential to improve therapies with highly potent active substances like nucleic acids through a spatially controlled mode of action in a tissue (Talebian et al., 2023). These implantable delivery systems for nucleic acids additionally benefit from

* Corresponding author.

E-mail address: christian.woelk@medizin.uni-leipzig.de (C. Wölk).

<https://doi.org/10.1016/j.ijpharm.2025.125330>

Received 20 November 2024; Received in revised form 27 January 2025; Accepted 6 February 2025

Available online 14 February 2025

0378-5173/© 2025 The Authors. Published by Elsevier B.V. This is an open access article under the CC BY license (<http://creativecommons.org/licenses/by/4.0/>).

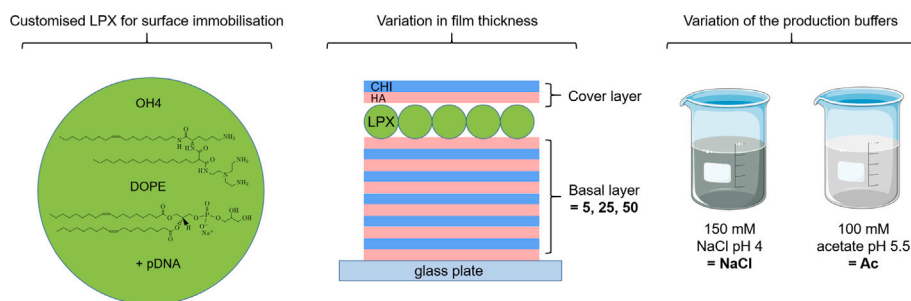


Fig. 1. Illustration of the concept of the studies. LPX composed of the ionizable lipid OH4 and the co-lipid DOPE were embedded in PEMs manufactured in different media and with increasing number of polyelectrolyte bilayers in the basal layer.

a prolonged local release of the genetic cargo. One example of a local nucleic acid delivery system are implantable biomaterials that allow an accurate spatiotemporal release of therapeutic nucleic acids in the field of cartilage regeneration (Yang et al., 2020). Such implantable delivery systems can be hydrogel-based or solid scaffold-based. For the latter systems, surface functionalization of the scaffold with nucleic acid carriers is a potential way of nucleic acid cargo loading. Within the various possibilities to realize surface attachment of macromolecular therapeutics, the Layer-by-Layer (LbL) approach has been proven beneficial (Hautmann et al., 2024). This strategy is based on the formation of polyelectrolyte multilayers (PEM) by the alternating deposition of oppositely charged polymers on surfaces (Su et al., 2009). Even though it is a simple and cost-effective technology, the LbL approach offers the possibility of creating versatile nano-structured functional materials with precisely controlled composition and structure, allowing for very accurate tailoring of the properties of the surface coating (Borges and Mano, 2014). Consequently, there are multiple possibilities for the functionalization of surfaces with nucleic acids using materials fabricated by the LbL technique (Linnik et al., 2021).

The simultaneous modification of the surfaces of scaffolds or implants through the application of LbL coatings and their functionalization by the immobilization of nucleic acids is considered especially attractive (Talebian et al., 2023). Conceivable applications for these types of surface coatings include the functionalization of stents for the prevention of restenosis and stent thrombosis (Hossfeld et al., 2013) and the modification of sutures (Castleberry et al., 2016; Chou et al., 2021). The strategy was also applied to modify wound dressings for the treatment of chronic non-healing wounds (Berger et al., 2023). Applications for the encapsulation of cochlear implants (Wey et al., 2021) and intraocular lenses (Wang et al., 2023) to counteract difficulties after implantation are also contemplated. According to the diversity of possible uses, substantially different characteristics are required for such multilayer systems.

Furthermore, the efficiency of LbL coatings for gene delivery does not only depend on the properties of the PEM and the interaction with the surrounding tissue, but the incorporated nucleic acid delivery system also plays a central role. Since it facilitates the nucleic acid uptake into the cell, the selection of a suitable delivery system for the nucleic acid is of decisive importance for the success of the therapy. Currently, virus-based vectors appear as the most established in clinical studies, although the disadvantages of these systems such as possible carcinogenic potential and the tendency to cause strong immune reactions in patients are well known (Fus-Kujawa et al., 2021). Dimitrova et al. demonstrated that it is generally possible to embed bioactive adenoviral vectors in LbL coatings (Dimitrova et al., 2007). Nevertheless, this approach has not prevailed, and chemical non-viral delivery systems are employed far more frequently as the transfection-active component in LbL-films.

Initially, it was attempted to directly incorporate the nucleic acid as the polyanion in LbL-films (Flessner et al., 2011; Saurer et al., 2013; Zou et al., 2014). However, degradation of PEM systems designed

in this way often leads to the formation of nano-sized nucleic acid-polycation complexes (Xie et al., 2018; Demuth et al., 2013), which subsequently serve as transfection vectors. As the formation of these nucleic acid-polycation nanoparticles is uncontrolled, it does not appear to be ideal for therapies with nucleic acids that need to be highly reproducible.

With cationic and ionizable lipids offering an appealing option for transfection systems due to their versatility and cost-effectiveness, they currently represent the most attractive non-viral transfection vectors (Ponti et al., 2021). However, there have only been few published attempts with substrate-mediated gene delivery by lipofection. Two initial methodologies were explored, both employing a primary LbL sequence comprising multiple layers of lipid-complexed DNA paired with layers of 'naked' DNA (Yamauchi et al., 2006) or layers of hyaluronic acid (Liu et al., 2011). These two systems focused heavily on the DNA itself as a coating component. Subsequently, Holmes et al. Holmes and Tabrizian (2013), Holmes et al. (2014) modified the strategy by introducing a technique based on an LbL-film of two polymers, hyaluronic acid and chitosan, with a single layer of embedded lipid nanoparticles. The described systems share a common feature: the utilization of lipofectamine 2000, a commercially available transfection reagent, as the transfection-active lipid component.

The approach to combine the beneficial properties of biopolymers in surface coatings with their use as lipid-based nucleic acid delivery systems was addressed in our research group, leading to the development of two new gene-functionalized surface coating systems incorporating lipoplexes (LPX). The active components of the LPX were newly designed ionizable lipids. One LbL-film design consisted of hyaluronic acid (HA) and chitosan (CHI), while the other consisted of chondroitin sulfate and collagen. Both approaches were published in proof-of-concept studies and provide different advantageous characteristics (Husteden et al., 2023, 2020a).

The study presented herein focuses on advancing the system comprising HA and CHI. Both of the utilized polymers are derived from natural sources and offer beneficial attributes for medical use, including biocompatibility, biodegradability, and absence of immunogenicity (Knopf-Marques et al., 2016; Bernkop-Schnürch and Dünnhaupt, 2012). In addition, both polymers have a monograph in the European Pharmacopoeia, which simplifies their subsequent translation to clinical application (Anon, 2023a,b). Notably, the employed CHI is recognized for its antibacterial properties (Hautmann et al., 2022; Rabea et al., 2003), and the synergy with HA, known for its anti-inflammatory effects (Alkhoury et al., 2020; Alkhoury et al., 2020; Altman et al., 2019), presents a particularly advantageous combination. Paving the path to preclinical *in vivo* transfer of the technique, this work focus on improving the manufacturing process of HA/CHI PEMs with embedded LPX composed of the newly designed ionizable lipid OH4 in combination with the established co-lipid DOPE (Fig. 1). As the proof-of-concept studies were performed using a time consuming pipetting approach, which is unfavourable for clinical application, improvements were required. We address an automatized production process allowing for the coating of complex structures. The surface coating based on

HA and CHI was systematically investigated to develop an automatized manufacturing of PEMs with increasing layer number using a dipping approach.

Different process parameters were varied as demonstrated in Fig. 1 and the resulting PEMs characterized according to surface topology. The main focus was to understand the effect of LbL-film properties on the quality and quantity of LPX incorporation. It was possible to identify manufacturing conditions suitable to prepare LPX-functionalized HA/CHI-PEMs. Finally, the functionality of the PEM was successfully proven by transferring reporter genes into cells using different experimental setups, either based on direct cell-PEM contact, or a contact-free setup in presence of hyaluronidase. These experiments also elucidate the mechanism of LPX release from the PEM. Summarizing, we present a highly versatile and adaptable system for local nucleic acid delivery and contact-mediated transfection.

2. Materials and methods

2.1. Materials

Except when indicated otherwise, all chemicals were purchased from Sigma-Aldrich (Taufkirchen, Germany). The phospholipids 1,2-di-(9Z-octadecenoyl)-sn-glycero-3-phosphoethanolamine (DOPE) and 1,2-di-(9Z-octadecenoyl)-sn-glycero-3-phosphoethanolamine-N-(lissamine rhodamine B sulfonyl) (ammonium salt) 18:1 (Rhod-DOPE) were obtained from Avanti Polar Lipids (Alabaster, USA). The ionizable lipid N-{6-amino-1-[N-(9Z)-octa|dec-9-enyl|amino]-1-oxo|hexan-(2S)-2-yl]-N'-(2-[N,N-bis(2-amino|ethyl)|amino]|ethyl)-|2-| hexadecyl|propan|di|amide (OH4) was synthesized in our group using established methods (Janich et al., 2014). Sodium hyaluronate (HA) (MW \approx 1.3 MDa) was provided by Kraeber & Co GmbH (Ellerbek, Germany) and Chitosan 85/500 (CHI) (MW \approx 0.2-0.4 MDa, degree of deacetylation \approx 85%) by Heppe Medical Chitosan GmbH (Halle, Germany). The pCMV-GFP plasmid, encoding for the reporter gene for expression of green fluorescent protein (GFP), was acquired from PlasmidFactory GmbH (Bielefeld, Germany). The GeneRuler 1 kb DNA-Ladder and TriTrack DNA Loading Dye (6X) were purchased from Thermo Fisher Scientific (Darmstadt, Germany).

2.2. Preparation of cationic liposomes

Lipid stock solutions (2 mg/mL) of OH4 (Janich et al., 2015) and DOPE were prepared separately with chloroform/methanol (8:2 V:V) as solvent and combined to a molar ratio of 1:1. A rotary evaporator was used to remove the organic solvent at 500 mbar for 30 min, followed by further drying of the lipid film at 10 mbar for 1.5 h. Afterwards, sterile filtrated 0.1 M sodium acetate buffer (pH 5.5) was added to the dried lipid film to yield a final total lipid concentration of 1 mg/mL. The lipid dispersion was shaken at 1400 rpm for 30 min using an Eppendorf ThermoMixer C (Eppendorf SE, Hamburg, Germany) and subsequently sonicated at 37 kHz for 15 min using an Elmasonic P sonication bath (Elma Schmidbauer GmbH, Singen, Germany), both at 50 °C. The liposomes were stored at 4 °C for up to one month and sonicated at room temperature for 5 min before LPX preparation.

2.3. Lipoplex preparation

The preparation of LPX was carried out by adding the plasmid DNA (pDNA) to the cationic liposomes in one step at a N/P ratio of 4 (ratio of primary amines of OH4 - N - to phosphate groups of the nucleic acid - P) in sterile filtrated 0.1 M sodium acetate buffer (pH 5.5). LPX of other N/P ratios were prepared for complexation studies. After combining the components by gentle pipetting, the LPX preparation was incubated for 15 min at room temperature while shaking at 300 rpm on an Eppendorf ThermoMixer C (Eppendorf SE, Hamburg, Germany). After complexation, the LPX dispersion was diluted to 300 μ L per well (24 well plate) with the associated buffer, depending on the preparation of the basal PEM.

2.4. Nanoparticle characterization

Particle size measurements were carried out by dynamic light scattering (DLS) using a Litesizer 500 (Anton Paar GmbH, Austria) and quartz cuvettes at 25 °C in 90° side scatter. The hydrodynamic diameter and the polydispersity index were derived from the correlation function by the Stokes–Einstein equation assuming a solvent viscosity of 0.890308 mPa s using the Kalliope software. The same instrument was used for electrophoretic light scattering (ELS) in Omega cuvettes (Mat.No. 225288). The zeta potential ζ was calculated using the Smoluchowski equation with the Kalliope software. For both measurements, the samples were adjusted to 20 μ g(total lipid)/mL for liposomes and LPX.

2.5. Polyelectrolyte solutions

The polyelectrolyte solutions have been prepared the day before PEM assembly at a concentration of 2 mg/mL, stirred overnight and sterile filtered before use. Polyethylenimine (PEI, MW \approx 750 kDa) was dissolved in 150 mM NaCl at pH 7.4. CHI and HA were dissolved in two different media to investigate the influence of the preparation buffer on the properties of the formed films: (i) 0.15 M NaCl solution adjusted to pH 4 using hydrochloric acid and (ii) 0.1 M sodium acetate buffer pH 5.5 (Fig. 1).

2.6. Basal PEM formation using a LbL dipping protocol

The basal PEM-films have been prepared using the DR 0 Layer-by-Layer deposition robot (Riegler & Kirstein GmbH, Potsdam, Germany) driven by Dipp3dWin software by alternating incubation of the substrates in either HA or CHI solution. If not stated otherwise, the used model substrates were circular glass cover slips with a diameter of 13 mm and a height of 0.13–0.16 mm (Karl Hecht GmbH & Co KG, Sondheim vor der Rhön, Germany). The substrate-holder illustrated in Fig. 2 has been custom designed and 3D-printed (material polylactide) to fix the cover slips during the LbL dipping procedure. The first immersion step of the substrates has been performed in the PEI solution for a duration of 15 min, followed by a washing step of 2.5 min. The washing solution media were identical to the media in which the polyelectrolytes were dissolved. Finally, the substrates were alternatingly incubated in either HA or CHI solution for 5 min, with intermediate washing steps for a period of 2.5 min between the polyelectrolyte incubations. The films were produced with 5, 25 and 50 HA/CHI-bilayers, as emphasized in Fig. 1, and terminated with one additional layer of HA to provide a negative surface charge for LPX adsorption. The films were stored in the preparation buffer in 24 well plates at 4 °C in the fridge. To avoid microbiological contamination for cell culture, the films were incubated in 70% (V/V) ethanol (AppliChem GmbH, Darmstadt, Germany) in Dulbecco's PBS (AppliChem GmbH, Darmstadt, Germany) for 10 min and subsequently rinsed with PBS two times.

2.6.1. Lipoplex deposition on PEM-films

The diluted LPX dispersion was pipetted onto the PEM-films in the 24 well plate and incubated for 2 h on the 3D rocker shaker at 8 speed/tilt (VWR International GmbH, Darmstadt, Germany). The applied volume of the LPX dispersion accounted 300 μ L per well and the concentrations were set to 1.3 μ g/mL total DNA for a aspired loading density of 0.3 μ g/cm² and 4.33 μ g/mL total DNA for a aspired loading density of 1 μ g/cm². The films were then washed twice with the respective production buffer. An additional cover layer was applied to the PEM-films on top of the LPX layer if not stated otherwise. For this purpose, in a first coating cycle 300 μ L of HA solution and in a second coating cycle 300 μ L of CHI solution were pipetted onto the PEM-films, incubated for 10 min and washed twice in between.



Fig. 2. Custom designed substrate holder made from polylactide for polyelectrolyte immersion of glass scaffolds.

2.7. Quantification of the nucleic acid cargo on the PEM-films

The nucleic acid cargo of the films was determined indirectly via the concentration of pDNA in the supernatant after the adsorption steps of LPX on the PEM-films. For this purpose, the supernatant of the LPX deposition step and the corresponding wash solutions were collected. The samples of the wash solutions were combined for analysis. For decomplexation of LPX (release of pDNA for quantification), a 30 mg/mL heparin solution (sodium heparin from porcine intestinal mucosa, ≥ 180 USP units/mg (standard unit of drug potency used in the United States Pharmacopeia), Sigma-Aldrich) was prepared in PBS pH 7.4 and mixed with the samples to a final concentration of 2 $\mu\text{g}/\mu\text{L}$ heparin in the samples, and samples were shaken for 5 min at 1500 rpm. Afterwards, samples were mixed with the same volume of ice-cold isopropanol to precipitate the pDNA and incubated for 20 min at -20 °C. After centrifugation at 21.300 g for 10 min at 4 °C, the liquid was carefully removed from the samples and the resulting pellet was gently washed in 500 μL of ice-cold ethanol. Then the ethanol was removed and the samples were resuspended in water (pH 8). The loading dye was added, and the samples were applied to agarose gels. The gels were prepared at 1% in TAE buffer with thiazol-orange. A 1 kB DNA ladder was applied for assessment as well as freshly prepared LPX which were treated in the same way as the samples to obtain a calibration for the sample quantification. The electrophoresis was performed for 1 h at 120 V. Gels were analysed using a GelDoc Go Imaging System (Bio-Rad Laboratories, Hercules, USA).

2.8. Fluorescence labelling of LPX

To assess the distribution of the LPX on the PEM-films, both a fluorescence-labelled lipid and fluorescence-labelled pDNA were used as tags. In order to obtain fluorescently tagged liposomes, Rhod-DOPE ($\lambda_{max}^{ex} = 560$ nm and $\lambda_{max}^{em} = 583$ nm) dissolved in chloroform/methanol (8:2 V:V) to a concentration of 2 mg/mL was added to the stock solutions for liposome preparation in the molar ratio OH4/DOPE/Rhod-DOPE of 1:1:0.002 (n/n) before the organic solvent was removed, and liposomes were prepared following the protocol mentioned above. Covalently Cy-5-labelled pDNA (Cy-5-DNA) ($\lambda_{max}^{ex} = 649$ nm; $\lambda_{max}^{em} = 670$ nm) was generated using the Label IT Nucleic Acid Labelling Kit from Mirus (Madison, USA), according to the manufacturer's instructions. Tagged LPX were fabricated using Cy-5-DNA and/or Rhod-DOPE-tagged liposomes or both for the LPX preparation instead of unlabelled components. The PEM-loading with fluorescence-labelled LPX was performed according to the established protocol.

2.9. Confocal laser scanning microscopy (CLSM) for distribution assessment of lipid and DNA on the PEM-films

For CLSM analysis, the PEMs with fluorescence-labelled LPX were used. The samples were subjected to three rinsing steps with the respectively used preparation buffer and afterwards fixed to a glass slide using Aquatex mounting medium (Merck, Darmstadt, Germany). The films were stored overnight at 7 °C for curing the mounting medium and subsequently examined using a LSM 710 (Carl Zeiss, Oberkochen, Germany).

2.10. LPX distribution assessment on the PEM-films using a laser scanner platform

A Typhoon™ laser-scanner platform (Cytiva, Marlborough, USA) was used for the evaluation of the surface coverage with LPX. LPX-loaded PEMs were prepared with the above described protocol using fluorescently tagged LPX. The selected resolution corresponded to 25 $\mu\text{m} \times 25 \mu\text{m}$ per pixel. For each preparation condition, 3 glass plates were coated with PEM embedded with Rhod-DOPE tagged LPX. As negative control the same samples were prepared with unlabelled LPX. The measuring conditions were kept constant for samples and controls.

2.11. Profilometry

Optical profilometry was conducted utilizing a laser scanning microscope model VK-X1050 (Keyence, Osaka, Japan) for the assessment of film surface topography and thickness determination. Therefore, PEMs were assembled on silicon wafers cleaned using the RCA protocol (Reinhardt and Kern, 2018). The analysis utilized a red laser emitting at 661 nm in reflection mode. Hydrated samples were positioned on a slide, and a segment was carefully sliced with a razor blade to ensure a flat edge for precise height measurement additional to topology. Along the generated edge, the height was determined at three defined points (same position for every sample to ensure an unbiased selection).

2.12. Static water contact angle (WCA)

Measurements were carried out using a drop shape analyser DSA25 driven by ADVANCE software (KRÜSS GmbH, Hamburg, Germany). The water drop application occurred on hydrated PEM-films with briefly dried surfaces and each measurement lasted 60 s, with one measured value recorded per second. The water contact angle was determined on both sides of the deposited droplet and the mean value was calculated.

2.13. Cell culture

Human embryonic kidney cells (HEK 293) were purchased from DSMZ (Deutsche Sammlung von Mikroorganismen und Zellkulturen, Braunschweig, Germany). The HEK 293 cells were maintained at 37 °C in a humidified 5% CO₂, 95% air atmosphere in high-glucose Dulbecco's modified Eagle's medium (DMEM) supplemented with 10% fetal bovine serum (FBS) and 1% Penicillin-Streptomycin. In order to maintain the cells below 80% confluence in a T75 cell culture flask, they were passaged every three days. A Trypsin/EDTA solution was used to detach the adherent cells. Cells were used up to passage 13.

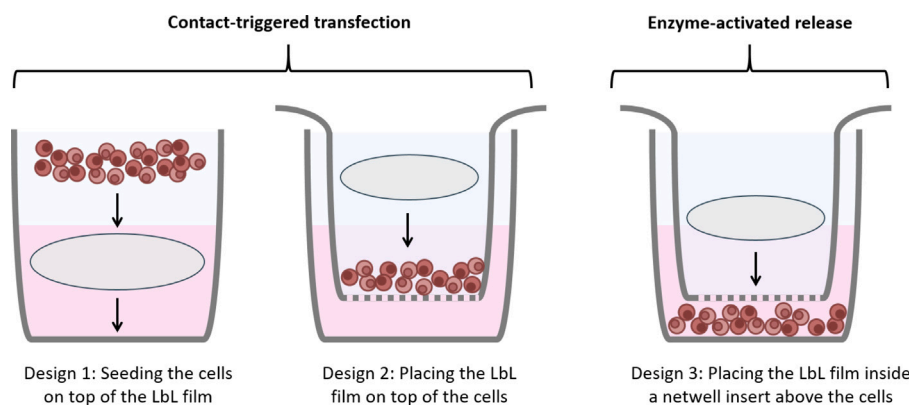


Fig. 3. Experimental setups for *in vitro* functionality testing of the LPX-loaded LbL-films.

2.14. Proliferation assay

For testing cell proliferation, the PEM coated glass coverslips (different LPX-loaded PEM films NaCl 5, 25, 50; Ac 5, 25, 50 were used with a theoretical maximal DNA loading rate of $1 \mu\text{g}/\text{cm}^2$) were placed in a 24 well plate with the LPX-functionalized PEM on top. Afterwards, they were treated with 300 μL of vitronectin XF (StemCell Technologies, Vancouver, Canada) solution diluted with PBS to a concentration of 20 $\mu\text{g}/\text{mL}$, followed by washing with PBS, to facilitate cell attachment. Then, 60 000 HEK cells per well were seeded on top of the PEMs (Design 1 Fig. 3). As positive controls, cells were seeded on the bottom of the well plate using the same conditions. The cells were incubated in 300 μL medium for 4 days and the medium was changed after one and two days. After 24, 48 and 96 h, 30 μL of alamarBlue cell viability reagent (Invitrogen, Waltham, USA) was added to the cells and incubated for two hours. Subsequently, 100 μL of the medium was transferred into a black flat-bottom 96 well plate and the fluorescence was determined at $\lambda_{\text{max}}^{\text{ex}} = 560 \text{ nm}$ and $\lambda_{\text{max}}^{\text{em}} = 590 \text{ nm}$ using a Synergy H1 plate reader (BioTek, Winooski, USA).

2.15. Contact-based transfection studies

For contact based transfection of cells, two different setups were used (Design 1 and 2, Fig. 3), both enabling a direct interaction of cells with the LPX-loaded LbL-films with a theoretical maximal DNA loading rate $1 \mu\text{g}/\text{cm}^2$. For transfection experiments using design 1, the experimental setup was equivalent to the proliferation assay, with the difference that the cell culture was kept for 5 days and instead of alamarBlue incubation cells were screened for GFP expression with the fluorescence microscopes Nikon eclipse TE2000-S (Nikon, Tokyo, Japan) or BZ-X800 (Keyence, Osaka, Japan) for stitching purposes. For design 2, 60 000 HEK cells per well were seeded into transparent 6 well transwell inserts with $0.4 \mu\text{m}$ pore diameter and a pore density of $2 \cdot 10^6$ pores/ cm^2 (TC Inserts SARSTEDT, Nümbrecht, Germany) to allow cell nutrition supply with the PEM-coated glass plate on top. The inserts were placed inside the well plates and equilibrated with 2 mL medium inside the insert and 3 mL medium outside the insert 30 min before cell seeding. Cells were seeded and cultured in the inserts for one day before the PEM-coated glass plates were placed on top of the cells (LPX-functionalized side facing cells). The PEM-film coatings were prepared according to the established protocol and no additional treatment with vitronectin was conducted. The cells were incubated for up to 5 days before readout. As positive control, suspension transfection was conducted by pipetting undiluted LPX corresponding to 1.3 μg pDNA per insert directly into the insert. Cells were screened with an inverted fluorescence microscope TE2000-S (Nikon Corp., Tokyo, Japan) and the fluorescent lamp C-HGFI (Nikon Corp., Tokyo, Japan) for GFP expression.

2.16. Transfection studies with enzymatic LPX release

The experiments were conducted according to design 3 (Fig. 3), a setup which allowed quantification via flow cytometry. 100 000 HEK cells per well were seeded in a 6 well plate in 3 mL cell culture medium. Type I-S hyaluronidase from bovine testes (400–1000 units/mg solid) was dissolved in PBS in the concentration 10 $\mu\text{g}/\mu\text{L}$ and added to the cells to the final concentrations of 10, 50 and 200 $\mu\text{g}/\text{mL}$. The glass plates coated with LPX-loaded PEM-films with a theoretical maximal DNA loading rate $1 \mu\text{g}/\text{cm}^2$ and with or without cover layers were placed with the LPX-functionalized side facing the mesh bottom of a $440 \mu\text{m}$ pore size netwell insert (Corning, NY, USA). These inserts were placed above the cells inside the cell culture medium without direct cell-PEM contact. Cells and PEM-films were subsequently incubated for 72 h together. As a positive control, a suspension transfection was performed by pipetting undiluted LPX corresponding to 1.3 μg pDNA directly into the wells. Following to the incubation period, the netwell inserts and therefore the PEMs were removed. The cell culture medium was removed as well and stored separately. The cells were detached using 0.5 mL Trypsin/EDTA solution for 5 min at room temperature and the medium removed prior was added to stop the reaction. Cells were centrifuged at 250 g for 5 min and the resulting pellet was resuspended in 200 μL PBS. The cells were stored on ice until analysis using a FlowCytometer (BD[®] LSR II Flow Cytometer, Becton, Dickinson and Company, Franklin Lakes, USA). The data was processed using FlowJo (version 10). Cells were gated by size (FSC-A) and granularity (SSC-A), and duplets were excluded from analysis by single-cell gating (FSC-H vs. FSC-A). The gate for GFP-positive cells was set according to the negative control.

2.17. Statistical analysis

The sample size is given as n below the corresponding figure. Data were statistically processed using GraphPad Prism software Version 10.4.0 (GraphPad Software, Boston, USA) without normalization. Statistical outlier tests using the ROUT method (Motulsky and Brown, 2006) were conducted for WCA data. Results are reported as mean \pm standard deviation (SD). Two-way ANOVA with a post-hoc Tukey test was used to check for statistical significance. Statistical significance is shown by asterisks in the figures.

3. Results

3.1. Characterization of the LPX

Proof-of-concept studies demonstrated that the pre-formation of LPX prior to LbL deposition was the most favourable protocol to incorporate lipid-complexed DNA into PEM-films (Husteden et al., 2020a). LPX were prepared according to a well established protocol from cationic

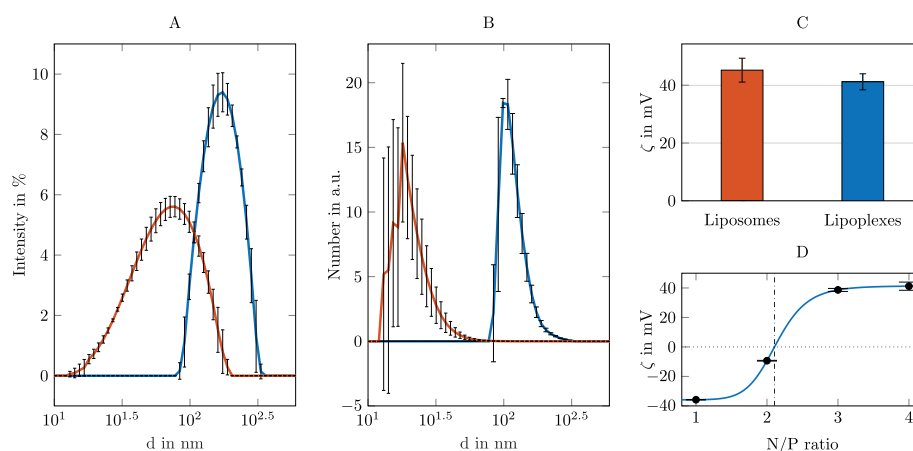


Fig. 4. Intensity-weighted (A) and number-weighted (B) size distribution curves and zeta potential (C) of OH4/DOPE liposomes (red) and LPX (N/P 4) (blue); Zeta potential as a function of the N/P ratio of LPX with sigmoidal curve fit with $r^2 = 0.9986$ (D). All measurements were executed in 0.1 M sodium acetate buffer at pH 5.5. Results are given as mean and SD of three measurements ($n = 3$).

liposomes (Janich et al., 2017). To facilitate the translation of the proof-of-concept of LPX-functionalized PEM-films to a clinically applicable system, the formulation buffer of LPX was exchanged from a MES buffer to an acetate buffer. MES is an accepted buffer in drug formulation, but it is more commonly used in molecular biology. In comparison, acetate buffer is a regularly used and well-accepted buffer in pharmaceuticals, and its components acetic acid and sodium acetate are FDA listed GRAS ingredients.

The cationic liposomes prepared in acetate buffer (100 mM pH 5.5) were characterized using DLS, resulting in a mean hydrodynamic diameter of 62.9 nm (SD = 0.5 nm) and an averaged PDI of 0.25 (SD = 0.006) indicating a broad, monomodal particle size distribution (Fig. 4). After LPX formation at N/P 4 the particle size distribution became narrower and the hydrodynamic diameter increased to 174.6 nm (SD = 1.1 nm) with a PDI of 0.15 (SD = 0.013). Additionally, the mean zeta potential of 45.2 mV (SD = 4.1 mV) for liposomes decreased to 41.2 mV (SD = 2.8 mV) after LPX formation with pDNA at N/P 4. The positive zeta potential enables electrostatic adsorption of the LPX on negatively charged surfaces during LbL deposition for PEM-film fabrication.

For monitoring the pDNA complexation in acetate buffer, the liposome formulation OH4/DOPE was incubated with pDNA at different N/P ratios and the zeta potential was measured. As demonstrated in Fig. 4, the zeta potential of LPX was a function of the N/P ratio and can be described by a sigmoidal curve. The sigmoidal fit resulted in an isoelectric point ($\zeta = 0$) of N/P 2.1, a value that is only slightly different from the value obtained in MES buffer ($\zeta = 0$ in MES was at N/P 2) (Janich et al., 2015). N/P ratios below the isoelectric point indicate LPX formulations insufficient for total DNA complexation. N/P ratios above the isoelectric point resulted in a plateau with positive ζ values. The relevant formulation of N/P 4 is in this positive plateau region. It can be assumed that the pDNA is quantitatively complexed and the LPX dispersion is colloidally stable at N/P 4.

3.2. Characterization of LPX-functionalized PEM-films

Since the objective of this study was to achieve uniform coatings of larger structures in an automated process which also allows for deposition of high layer numbers, certain parameters of the previously reported production process needed adjustment. The acquisition of a dipping robot was an essential step enabling automated parameterized manufacturing of the LbL coating, a prerequisite for the later planned transfer to structures with different surface geometries as well as upscaling. Additionally, automated manufacturing allows for the production of free-standing LbL-films, which need dimensions of 25 or

more polyelectrolyte bilayers.

Further, we decided to test different LbL preparation buffers: isotonic saline solution at pH 4.0, as used in the proof-of-concept study (Husteden et al., 2020b), and 0.1 M sodium acetate buffer at pH 5.5, which is widely established in the fabrication of chitosan-based LbL-films (Sousa et al., 2023; Silva et al., 2015; Cunha et al., 2024; Rosas et al., 2024; Facchi et al., 2023). Consequently, two critical parameters of the LbL deposition technique, namely, ionic strength and pH value, were changed. Since both parameters influence the charge of polyelectrolytes, this can fundamentally alter the properties of the resulting PEM. For instance the degree of ionization of the polyelectrolyte and the ionic strength determine the polyelectrolyte conformation and the thickness of the PEM (Nascimento et al., 2018; Taketa and Beppu, 2014), which is why one focus of the investigation was set on surface topology, thickness and wettability. Further, polyelectrolyte charge and conformation may also influence LPX deposition, which was the reason for screening the quality and quantity of LPX embedding. The electrostatic interaction between HA and CHI is the main driving force for the PEM-film growth of the HA/CHI multilayer. With increasing pH value, the theoretical degree of ionization of HA, which has an assumed pKa of 3.0 according to literature (Anon, 2023b), increases, while it decreases for CHI with an approximate pKa of 6.5 (Anon, 2023a), as demonstrated in Fig. 5A. According to the Henderson–Hasselbalch equation, at pH 4 90.9% HA and 99.6% CHI are ionized, while that ratio is exactly inverted at pH 5.5. Consequently, we chose the following screening parameters (see also Fig. 1): (i) preparation buffer 0.1 M sodium acetate buffer pH 5.5 and 0.15 M isotonic saline solution pH 4. (ii) different number of deposited HA/CHI bilayer of the basal PEM (5, 25 and 50 bilayers). In the following text, the PEMs are designated according to their respective preparation buffers as Ac for the PEMs prepared in acetate buffer and NaCl for the PEMs prepared in saline solution with the suffix of a number indicating the number of double layers of the basal PEM. This nomenclature will be used throughout the article, but in particular in the illustrations like in Fig. 5.

3.2.1. Topological investigations

The film topology of hydrated PEMs is an important parameter to be investigated. Unfortunately, an attempt to use atomic force microscopy could not be realized successfully because of the thickness and swollen properties of the PEMs produced in acetate buffer (data not shown). Thus, optical profilometry was applied to characterize the PEM-film thickness and topology in the hydrated state. The results are summarized in Figs. 5B and 6. According to the topology, visualized in the microscopic profile images, all films have a certain roughness (Fig. 6). Structures with a pronounced height were observed, which

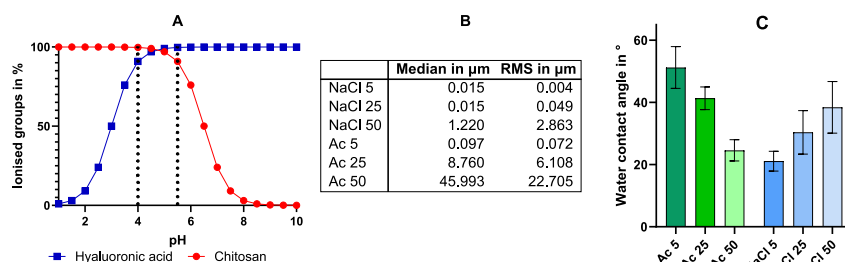


Fig. 5. Calculated theoretical degree of ionization of the polyelectrolytes obtained from the Henderson–Hasselbalch equation assuming the pKa values 6.5 for CHI and 3 for HA (A), Median and root mean square (RMS) value of the thickness of LPX-loaded PEM-films d obtained from optical profilometry (B) and static water contact angle results represented by mean and SD of 3 measurements ($n = 3$) which lasted 60 s with one obtained value per second, outliers were identified using the ROUT method (Motulsky and Brown, 2006) ($Q = 10\%$), Two-way ANOVA with Tukey's multiple comparison test indicated statistically significant differences for all samples with $p < 0.0001$ except from Ac 50 vs. NaCl 25 with $p = 0.0009$ (C).

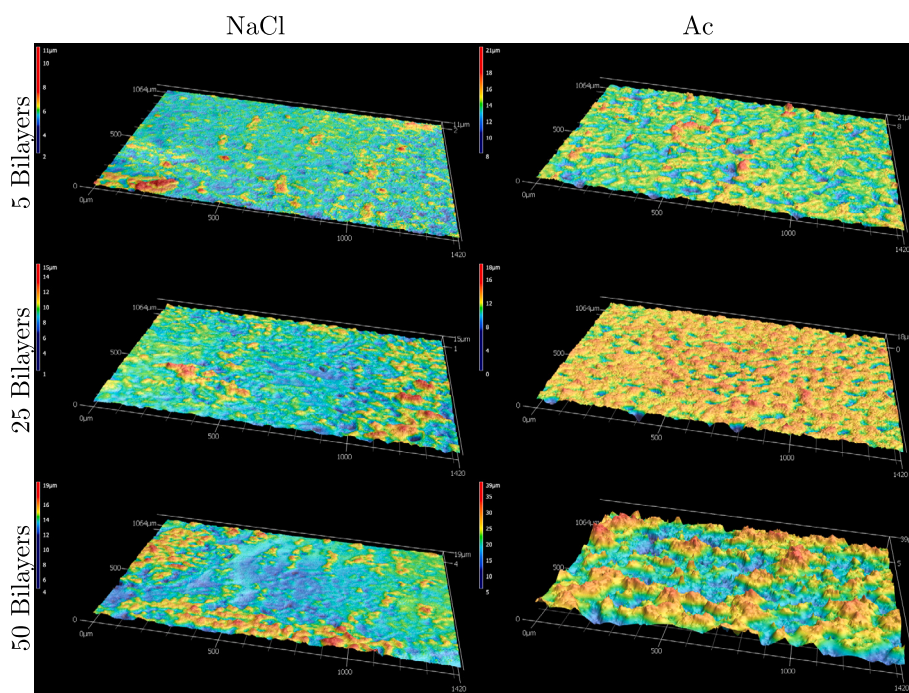


Fig. 6. Optical profilometry images of the hydrated LPX-loaded PEMs. The height scales and colouring are adapted to the individual films and their total thicknesses to obtain sensitivity for individual differences. The indicated number of bilayers corresponds to the basal PEM.

may indicate an island-like growth of LbL materials. This effect was most pronounced for the PEM prepared in acetate buffer with 50 HA/CHI bilayers (Ac 50), and less pronounced for the 25 bilayer system fabricated in the same buffer (Ac 25).

More insights were provided by the average height measurements (Fig. 5B). The median values of the thickness determination demonstrate that PEMs produced in acetate buffer are considerably thicker compared to the PEMs prepared in NaCl solution. PEMs prepared in NaCl solution are characterized by thickness values in the nm scale for low bilayer numbers (NaCl 5 and 25), and only NaCl 50 PEMs were characterized by a thickness of $\approx 1.2 \mu\text{m}$. PEMs prepared in acetate buffer are much thicker. The Ac 25 PEMs were already characterized by a height of $\approx 8.8 \mu\text{m}$. We also calculated the root mean square (RMS) values, where larger values of the population of the measured parameter have a stronger impact compared to the mean value calculation. However, the RMS also showed the same trends as the median evaluation.

3.2.2. Water contact angle measurements

The wettability of surfaces is a parameter which determines protein adsorption and cell adhesion. WCA measurements were carried out by

the sessile drop method using an optical tensiometer. As demonstrated in Fig. 5, all surfaces were found to be hydrophilic with WCAs below 90° . Thus, it can be assumed that the films provide good wettability. It should be noted that, beside the PEM film composition, the roughness of the films also has an influence on the wettability, as according to Wenzel (Wenzel, 1936). Different trends were observed for the PEM films fabricated in the different preparation buffers. For PEM-films prepared in acetate buffer, the WCA decreases and consequently the hydrophilic character increases with increasing number of deposited HA/CHI bilayers, while the WCA of PEM-films prepared in NaCl increases with increasing number of multilayers.

3.3. Characterization of LPX embedding in PEM-films

Preliminary tests using a quartz microbalance revealed a more stable binding of the LPX on the PEM-films produced in acetate buffer compared to those manufactured in the NaCl medium (data not shown). Based on this finding, LPX embedding was determined in more detail for the PEM films characterized above. In addition to the variation in basal PEM thickness and the preparation buffer, the LPX-loading

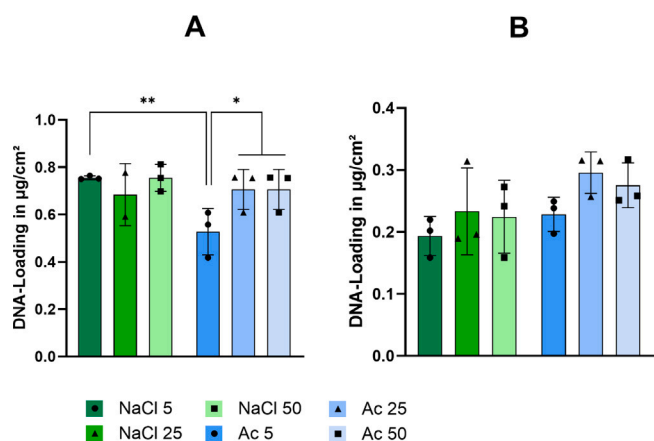


Fig. 7. Determination of loading of PEM-films with LPX cargo given in DNA amount in $\mu\text{g}/\text{cm}^2$ for a theoretical maximal loading of (A) $1 \mu\text{g}/\text{cm}^2$ and (B) $0.3 \mu\text{g}/\text{cm}^2$ assuming LPX incorporation of 100%. Results were determined indirectly by gel electrophoresis of loading supernatants and washing solutions with a sample size of $n = 3$ (* $p < 0.005$, ** $p < 0.05$).

rate of the PEM-films, given as DNA mass/area, was varied from $1 \mu\text{g}/\text{cm}^2$ (the standard concentration used above) to $0.3 \mu\text{g}/\text{cm}^2$ (a lower concentration to decrease the total dose of nucleic acid). This was done to investigate whether the loading dose has an influence on the quality of LPX deposition in order to take this into account in future development processes. Both loading rates were chosen because qualitative reporter gene expression in HEK cells was microscopically detected in preliminary experiments using transfection Design 1.3 (data not shown). At this development step the used amount of DNA is not connected to a specific clinical application.

An indirect quantification of LPX embedded in the PEMs was achieved by determining the pDNA content in the supernatant after the LPX deposition step. Attempts to perform a direct quantification with fluorescence-based methods in intact PEM-films or after PEM disintegration failed until the current time point due to low reproducibility or quenching effects (data not shown). The results of the indirect quantification are shown in Fig. 7. Analysis of the supernatant revealed no significant influence of the different formation buffers for the higher LPX loading rate of $1 \mu\text{g}/\text{cm}^2$, except for the Ac 5 films with significant lower loading capacity compared to Ac 25, 50 and NaCl 5. At a LPX loading rate of $0.3 \mu\text{g}/\text{cm}^2$, it was clearly noticeable that the PEM-films NaCl 25 and NaCl 50 showed increased standard deviations, and thereby lower reproducibility in LPX deposition, (Fig. 7B). The loading of the NaCl PEM-films was significantly increased in comparison to the Ac PEM films with $p \leq 0.018$, while no significant differences were detectable between the different PEM-film thicknesses. There was no pDNA detectable in any of the washing buffer solutions, indicating stable binding of the LPX after incubation. Images of the original electrophoreses for pDNA quantification can be found in the supporting information Figures S1 and S2.

CLSM investigations of LPX-loaded PEMs were used to get insights into the microscopic distribution of embedded LPX. For this investigation fluorescently-labelled LPX were used. It has to be considered that this method has a resolution limit for the size of detectable particles (calculated resolution: around 225 nm at a wavelength of 583 nm). The resolution does not allow the assessment of the individual LPX size, rather, aggregates and associates of LPX can be detected. The micrographs with co-labelled LPX (Cy-5-DNA and Rhod-DOPE tags) show a high degree of co-location of the signals of both labels for all film designs as exemplary illustrated in the supporting information (Figure S3). This indicates LPX integrity when embedded in the PEM. For better comparison, Fig. 8 exclusively displays the images that refer to the signal of Rho-DOPE LPX label. The LPX distribution in

the investigated PEMs was characterized by pronounced differences. PEMs produced in 150 mM NaCl pH 4 were characterized by larger LPX agglomerates in the PEM, with a tendency of less agglomeration on NaCl 50. Films manufactured in 0.1 M acetate buffer pH 5.5 showed only very small agglomerates, with a uniform distribution of LPX. Here the highest tendency for agglomeration was observed for Ac 50. Overall, the LPX distribution on the PEM-films Ac 5 and Ac 25 appears more uniform, with fewer agglomerates compared to the other PEM-films. Investigating the distribution of LPX over the entire surface of the PEM coated glass slides, Rhod-DOPE tagged LPX were used for analysis with a fluorescence laser scanner platform. In this experiment, the two different LPX loading rates were also selected ($1 \mu\text{g}/\text{cm}^2$ of DNA and $0.3 \mu\text{g}/\text{cm}^2$ of DNA). Representative images are shown in Fig. 9, and all measured triplicates are presented in the supporting information (Figures S4-S9). For PEM-films treated with the LPX loading rate of $1 \mu\text{g}/\text{cm}^2$, fluorescence was distributed over the entire surface and the films showed areas with higher fluorescence intensity. These were mainly located at the edge of the coverslips, but also in the centre. This effect was more pronounced in the PEMs prepared in acetate buffer. There were no significant differences between the investigated film thicknesses for the two production buffers. For PEMs treated with a LPX loading rate of $0.3 \mu\text{g}/\text{cm}^2$ fluorescence could also be recognized over the entire surface of all films, with some areas of very low intensity. The PEM-films Ac 5 and Ac 25 showed a ring structure of lower intensity, most probable an effect of the shaking movement during LPX incubation for loading. The analysis could demonstrate the quality of LPX embedding on the macroscopic scale, but can only be used to a limited extent for quantitative evaluations, due to possible quenching effects. In summary, an efficient surface coating was demonstrated, but due to the observed uneven distribution in the macroscopic scale, the LPX loading process has to be improved for ongoing applications.

3.4. *In vitro* biocompatibility studies

In order to study the biocompatibility of the PEM-systems, HEK 293 cells, which were also used for transfection studies, were seeded on top of the LPX loaded PEM-films with $1 \mu\text{g}/\text{cm}^2$ cargo and cultivated for up to 4 days. HEK cells were chosen as a common cell line used for lipofection screening. Cell proliferation was determined using a resazurin-based alamarBlue assay. The results are summarized in Fig. 10. On all tested PEM-film coatings a significant increase in metabolic activity with prolonged incubation time was detected within 4 days. Comparing the different PEM-films at the same time point showed no significant differences. It can be assumed that none of the films are specifically toxic to HEK 293 cells. The increase of the alamarBlue fluorescence intensity with time was also demonstrating cell proliferation of HEK cells on the different PEMs.

Although cell growth was not impaired significantly as demonstrated with the alamarBlue assay, the formation of larger, spheroid-like structures could be observed for HEK 293 cells on all PEM-films prepared in acetate buffer after 4 days, while the cell morphology on PEM-films prepared in NaCl remained unaltered. Exemplary images are shown in the supporting information (Figure S11). This might indicate that cell adherence was affected, driving the cells to form the spheroidal structures by increasing cell-cell contact. According to the observed higher thickness of three investigated Ac PEMs, indicating a more swollen polymer layer network, it can be assumed that these coatings are characterized by a softer gel-like structure which might explain the decrease of cell-surface interaction (Pahal et al., 2023). Nevertheless, mechanic investigations to prove the hypothesis of coatings prepared in acetate buffer being softer were not performed in this set of experiments.

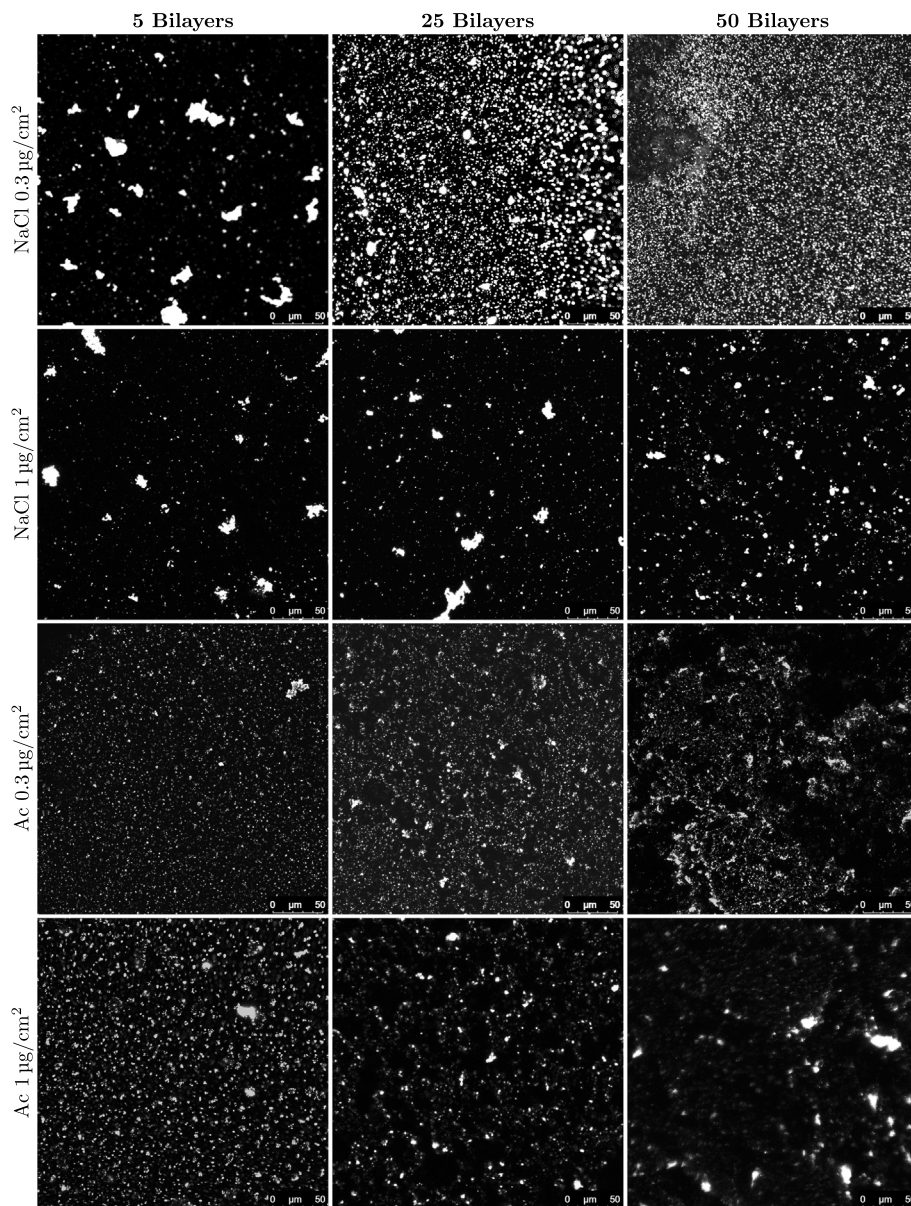


Fig. 8. Representative CLSM micrographs of LPX loaded PEM-films of varying basal layer thickness prepared in the different buffers. The presented images show the rhodamine signal of Rho-DOPE-tagged LPX. Every image has a dimension of $290 \times 290 \mu\text{m}$. The indicated number of bilayers corresponds to the basal PEM. The scale bar at the right bottom of each image represents $50 \mu\text{m}$. The labelling on the left gives the preparation buffer and hypothetical LPX loading rate (assuming LPX incorporation of 100%) as mass DNA per area for each line.

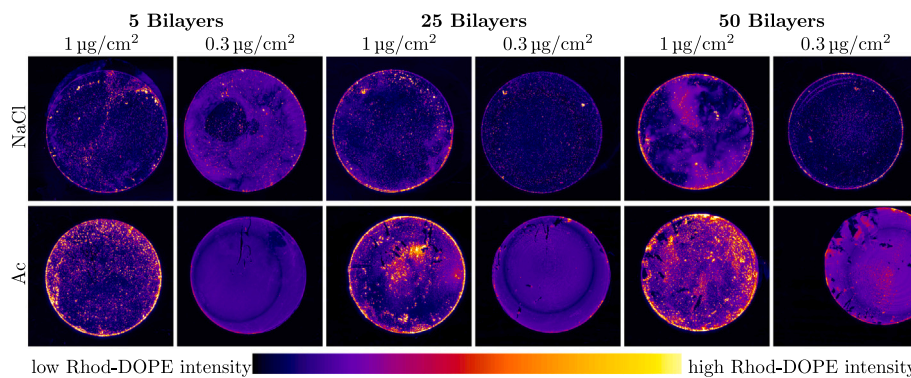


Fig. 9. Fluorescence scanner images of glass coverslips (diameter of 1.3 cm) coated with PEMs embedding Rhod-DOPE labelled LPX. The Rhod-DOPE fluorescence intensity, indicating LPX density, in the images is displayed in the LookUp Table Fire in ImageJ (intensity legend illustrated below the images). The loading rate label of the columns in $\mu\text{g}/\text{cm}^2$ gives the hypothetical LPX loading rate (assuming LPX incorporation of 100%) as mass DNA per area.

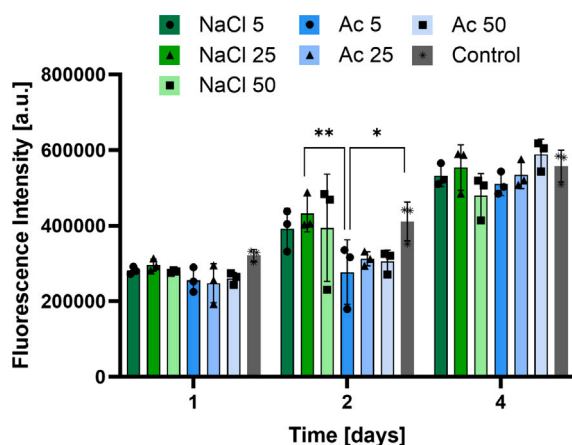


Fig. 10. *In vitro* proliferation assay for HEK 293 cells seeded on the different LPX-loaded PEMs (DNA loading rate $1 \mu\text{g}/\text{cm}^2$) determined by alamarBlue assay. The fluorescence intensity values correlate with the metabolic activity of cells. As a control, HEK 293 cells on cell culture dishes were used. The experiments were carried out as triplicates. Two-way ANOVA with Tukey's post-hoc test stated highly significant influence of the time $p < 0.0001$ (* $p < 0.05$, ** $p < 0.01$).

3.5. Functionality studies

3.5.1. Contact-triggered transfection

As mentioned above, HEK cells were used as an established screening cell line for transfection experiments. It was planned to determine the DNA-transfer activity of the LPX-functionalized PEM-coatings with cells seeded on top of the PEMs (Design 1 Fig. 3), using DNA encoding for GFP as reporter gene. Although direct seeding of cells on top of LPX-loaded films is only feasible for *ex vivo* applications, this setup was used because the proof-of-concept study demonstrated a contact-triggered transfection. For this purpose, the cells were seeded on the LPX-functionalized PEMs and incubated for several days. Due to formation of spheroidal cell associates, it was not possible to separate single cells and quantify the relative amount of GFP-positive cells by flow cytometry. Also, microscopic quantification was not practicable because the cells were located in different focal planes. Furthermore, it was not possible to quantitatively detach the HEK cells from all three investigated Ac PEMs. Consequently, evaluation was limited to qualitative microscopic analysis. Stitched microscopic images of the fluorescence of GFP-positive HEK 293 cells after 5 day contact with the PEMs are shown in the supporting information (Figure S13–S20). These images reveal the higher transfection potential of the PEM-systems prepared in acetate buffer. A looser, more swollen character of the AC PEM-films, indicated by the higher observed thickness when comparing NaCl with AC films with equal layer number, can explain the problem of cell detachment, and also a possible higher transfection rate. With a more swollen hydrated polymer chain network better penetration of cells into the structure, and consequently a higher accessibility of LPX, can be assumed. This finding, in combination with the results of the LPX deposition studies, the lower roughness of Ac 25 PEMs compared to Ac 50 PEMs and the additional observation that it was possible to detach the Ac 25 PEMs from the glass support (image of detached film in the supporting information Figure S10), lead us to the decision to focus on Ac 25 films for further characterization. Hence, the feature of PEM detachment is a necessary step to free-standing PEMs, a research direction we want to follow in future research. Consequently, we investigated Ac 25 PEMs in experimental design 2 (Fig. 3), which is also more relevant for the biomedical application of biomaterials placed in a tissue.

In order to investigate this contact-forced transfection, HEK cells were seeded in an insert which allowed them to grow on a stable surface with guaranteed nutrient supply. The LPX-loaded PEMs were

subsequently placed on top of the cell layer with the transfection-active side facing the cells. Furthermore, the films were prepared with and without cover layers on top of the LPX layer to assess their effect on the transfection efficiency. In this way, the cells could be transfected to a considerable extent. Microscopic images are presented in the supporting information (Figures S21–S29), with selected images being presented in Fig. 11. It was notable that GFP expression was clearly recognizable in the PEM-films without a cover layer after just one day, while the films with an additional cover layer only showed higher transfection rates after a few days. This indicates a delay which can be controlled by the thickness of the cover layer. However, actual quantification again proved to be problematic because quantitative cell detachment for flow cytometry was not possible once more. Due to the experimental setup and interference effects with the PEM, a microscopic quantification could also not be performed. Hence, based on this experiment, it can be assumed that the enzymatic environment of the cells may play a role for the release of LPX from the PEM-films that results in cell transfection, especially when LPX are embedded under a cover layer. Cell-derived hyaluronidase can be one of the possibly responsible enzymes.

3.6. Transfection experiments based on enzymatic release of LPX

Based on the research of Cardoso et al. (Cardoso et al., 2016), which indicated enzymatic degradation of LbL-films composed of HA and CHI by hyaluronidase, we decided to investigate the effect of the enzyme on LPX release. In a previous work, we proposed that enzymatic activity of cells may play a key role for LPX release and transfection (Husteden et al., 2023, 2020a). The kinetic difference in GFP expression of cells in contact with LPX-functionalized PEMs with or without cover layer described for the contact-forced transfection of design 2, see previous section, supports this hypothesis. In order to investigate a possible hyaluronidase-associated release of LPX from the films, cells were seeded in well plates and LPX-loaded PEM-films Ac 25 with and without a cover layer were placed in netwell inserts above the cells to exclude direct cell-PEM contact, as illustrated in design 3 in Fig. 3. Three different concentrations of the enzyme hyaluronidase, namely $10 \mu\text{g}/\text{mL}$, $50 \mu\text{g}/\text{mL}$ and $200 \mu\text{g}/\text{mL}$, as well as a control without the enzyme, were added to the cell culture medium. The results are depicted in Fig. 12. The results of the classical suspension transfection showed an effect of the enzyme on the efficacy. Significantly higher transfection rates of the samples treated with $10 \mu\text{g}/\text{mL}$ (72.3% GFP+ cells), $50 \mu\text{g}/\text{mL}$ (64.6% GFP+ cells) and $200 \mu\text{g}/\text{mL}$ (65.9% GFP+ cells) hyaluronidase were observed compared to the samples in absence of hyaluronidase, in which 33.7% of the cells showed GFP expression. Hence, hyaluronidase seems to effect OH4/DOPE-based lipofection in HEK cells.

Examining cells in the presence of Ac 25 with a cover layer indicates the reservoir mechanism of the PEM. In absence of hyaluronidase, 0.7% GFP-positive cells were detected, indicating almost no GFP expression. The LPX are embedded in the PEM-film due to the cover layer and are not available for transfection. In presence of hyaluronidase the transfection efficiency increases to 6.0% at $10 \mu\text{g}/\text{mL}$ and 4.1% at $50 \mu\text{g}/\text{mL}$. At the enzyme concentration $200 \mu\text{g}/\text{mL}$, the transfection rate increased significantly to 44.5%. These results demonstrate that embedding LPX in the PEM using a cover layer has a reservoir function, and hyaluronidase can release functional LPX from the PEM. This is supported by the final experimental group, where the cells were cultured below Ac 25 PEMs without a protective cover layer on top of the LPX. All samples showed clear transfection activity. The transfection rate was significantly higher in HEK cells in absence of hyaluronidase with 45.7% compared to the ones with $10 \mu\text{g}/\text{mL}$ (27.3% GFP+ cells), $50 \mu\text{g}/\text{mL}$ (20.5% GFP+ cells) and $200 \mu\text{g}/\text{mL}$ (26.2% GFP+ cells) supplemented enzyme. The results clearly show that in this group hyaluronidase is not necessary for LPX release. Physical desorption of LPX can occur under the experimental conditions and the LPX can

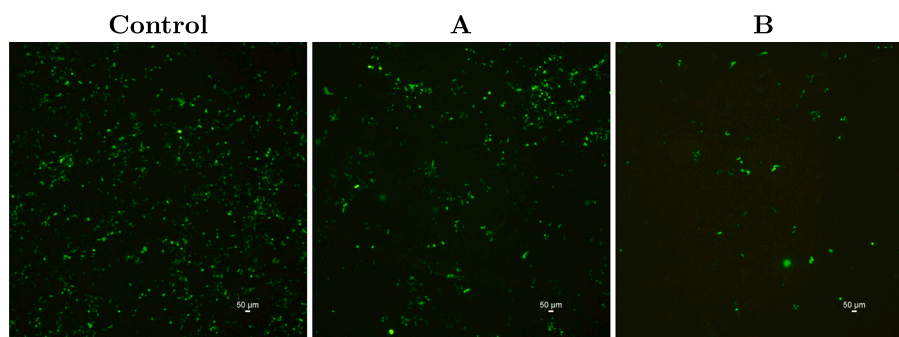


Fig. 11. HEK cells after 96 h of incubation in cell culture inserts with LPX containing 1.3 µg pDNA in the cell culture medium (Control), below glass slides corresponding to experimental Design 2 with Ac 25 films with the theoretical maximal LPX loading rate of 1 µg pDNA /cm² without a top layer (A) and with one additional bilayer as a cover layer (B). Further images are available in the supporting information Figure S21–S30.

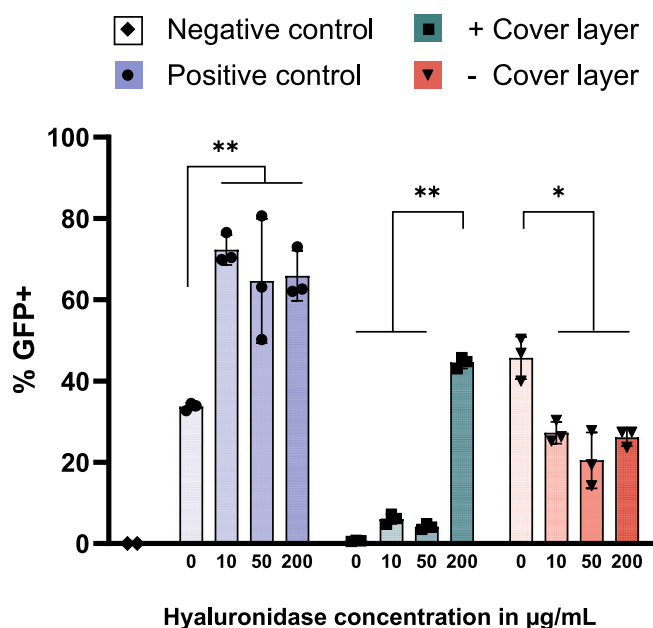


Fig. 12. Transfection efficiency determined by flow cytometry as % GFP-positive cells. HEK 293 cells were incubated with 0 µg/mL, 10 µg/mL, 50 µg/mL and 200 µg/mL hyaluronidase in the cell culture medium. The cells were treated with LPX containing 1.3 µg pDNA in suspension as a control or LPX-loaded Ac 25 PEM films (approximately 1.3 µg pDNA) with and without a HA/CHI cover layer for 72 h according to design 3 (Fig. 3). The experiments were conducted as triplicates (*p < 0.0025, **p < 0.0001). Two-way ANOVA with Tukey's post-hoc test.

diffuse to the cells in the bottom compartment. Nevertheless, the reduced activity in presence of hyaluronidase in the setup without cover layer indicates that digestion products (e.g. small molecular weight hyaluronic acid alone or in complex with chitosan) or hyaluronidase itself may interfere with the LPX desorption. In summary, the results presented here and in the previous section demonstrate that a cover layer is necessary to control the reservoir effect of the Ac 25 PEM coating and that hyaluronidase triggers the LPX release from the PEM system. Surprisingly, hyaluronidase also had an increasing effect on the simple suspension transfection, the mechanism behind which is unclear.

4. Discussion

In this study, the goal was to improve the strategy of LPX immobilization in LbL-coated surfaces in terms of implementation of a manufacturing process which is automatized and allows the coating

of larger surfaces. Examined key parameters were the LPX loading capacity and quality. We systematically screened the LbL preparation of HA/CHI PEMs with an automatic dipping approach in two different preparation media for basal layers with different thickness. As manufacturing media, we used 150 mM NaCl adjusted to pH 4 (medium used in the proof-of-concept study) and 100 mM sodium acetate buffer with pH 5.5. Consequently, pH and ionic strength were different. Notably, the pH shift had an effect on the ionization degree of the polyelectrolytes in solution as demonstrated in the calculated curve in Fig. 5A. Highly ionized polymer chains tend to be adsorbed with flat chain conformations and less ionized polymer chains with more loop and tail structures (Nascimento et al., 2018). Consequently, the film structure can be significantly affected. Moreover, the ionic strength affects PEM structures. Hernandez-Montelongo et al. were able to show that with increasing ionic strength the difference of the zeta potential of CHI in solution decreased, while an increase was observed for HA (Hernandez-Montelongo et al., 2020). Further, they demonstrated that film thickness was decreasing with increasing salt concentration. Taketa et al. investigated using AFM measurements and profilometry that a higher ionic strength resulted in rougher HA/CHI PEMs (Taketa and Beppu, 2014). This effect was discussed as a result of conformational changes in the polymers in solution induced by a higher ionic strength. This can also affect other film properties as well. Nascimento et al. observed that the films become more hydrophilic at lower preparation pH and ionic strengths. Our investigations reflect these findings. The PEMs prepared in 0.1 M acetate pH 5.5 are thicker and in a more swollen state compared to PEMs prepared in 0.15 M NaCl pH 4. This affected the cell adhesion, but not the amount of embedded LPX. The investigation of the quality of LPX embedding showed that a basal PEM fabricated in 0.1 M acetate pH 5.5 resulted in a more uniform LPX distribution with lower tendencies for aggregation. Because of this benefit, further focus was set on these PEMs. In transfection studies the efficacy was shown for PEMs in different setups. Hence, direct contact of cell layers with the LPX-embedding PEMs demonstrated efficient transfection of the reporter gene in the PEM into adjacent cells. The cover layer seems to play a key role for the reservoir function. Our experiments support the hypothesis that enzymatic degradation and cellular PEM remodelling drive the LPX release and consequently lead to efficient transfection. This has to be taken into account for possible clinical applications. The usability of PEM-films as biomaterials depends decisively on the film properties. For instance, the films presented herein are conceivable for use in the field of bone regeneration of critically size defects. For this application, a possible strategy can be the transfer of the PEM-film coating on biodegradable implants, where an efficient coating has to be evaluated for different implant geometries and materials. In such a scenario, functionalization with nucleic acids encoding for bone morphogenetic proteins is a possible scenario (Zhang et al., 2018). Also, the mechanical

characteristics of the PEM-films have to be optimized for application in the field of bone regeneration, as stiff surfaces are beneficial for the osteogenic differentiation of stem cells (Cipitria and Salmeron-Sanchez, 2017; Cantini et al., 2020). Since the stiffness is not determined in the present study, such measurements are required. In order to adjust the stiffness, chemical cross-linking strategies are a possible tool. Also, the characterization of protein adsorption and the interaction with mesenchymal stem cells will be a future task to transfer the system in such a direction. Another possible application field for the LPX-embedding PEM-films is the utilization as advanced functional wound dressing for chronic wounds. Here, the functionalization with nucleic acids encoding for growth factors promoting wound healing, or small interfering RNAs inducing gene silencing of inflammatory genes, are possible strategies using the LPX-functionalized PEMs (Boateng and Catanzano, 2015). Nevertheless, the PEMs have to be improved for this application. Adapting the system to provide soft, but mechanically resilient free-standing PEMs would be necessary. Cross-linking strategies are also needed to tune the mechanical stability. Further, the surface characteristics of the PEMs have to be investigated, and maybe improved, to yield balanced protein adsorption and cell adhesion. For the Ac 25 PEM characterized here, an application in which a direct contact between tissue and PEM can be guaranteed is possible. A benefit for efficient transfection can be expected from cells with hyaluronidase activity. For instance, hyaluronidase has a high activity in cancers (McAtee et al., 2014) and in bacterially infected wounds (Liu et al., 2024). An unexpected finding was that hyaluronidase also effects the efficiency of the suspension transfection with LPX in HEK cells. Two hypotheses can be made, but are not experimentally checked in this research. Hyaluronidase may change the glycocalyx properties of the cells resulting in an increased LPX-cell interaction which consequently promotes LPX uptake, or hyaluronidase-processed soluble HA fragments may interact with the LPX and induce surface properties which promote cellular internalization.

5. Conclusion and outlook

In this work, we describe the systematic investigation of LPX-loaded PEMs produced by a dipping protocol. The resulting Ac 25 PEM finally emerged as a promising and versatile system for localized delivery of therapeutic nucleic acids. It is possible to transfect cells which are in contact with the LPX-functionalized PEMs, although the LPX are embedded in the system by applying a cover layer. Hyaluronidase seems to play a key role to make the LPX accessible to cells. The PEM enables surface-mediated transfection of cells. Future aspects will focus on the possibility to transfer the system to flexible, support-free, mechanically resilient films for a possible application in wound management, or on evaluating the coating on porous scaffold structures for application in the field of bone regeneration. While the first research direction needs the optimization of the PEM thickness, the latter focuses more on the transfer of the dip-coating process of the AC 25 films, with a focus on the used scaffold material and porosity. Both directions may benefit from the development of a cross-linking strategy. Hence, the herein presented research reveals two required research fields. The LPX deposition technique would benefit from a directed deposition technique which enables a spatial controlled LPX embedding. Another required research field is the nucleic acid quantification directly in the film, ideally by a surface scanning method, to screen for the nucleic acid dose.

CRedit authorship contribution statement

Maria Krabbes: Writing – original draft, Visualization, Investigation, Formal analysis, Conceptualization. **Vincent Kampik:** Investigation, Formal analysis. **Jan Krieghoff:** Writing – review & editing, Visualization, Investigation, Formal analysis. **Vivian Haas:** Writing – review & editing, Visualization, Investigation. **Mathilde Heizmann:** Visualization, Investigation. **Maria Morawietz:** Investigation.

Hermann Kalwa: Resources, Investigation. **Leonard Kaysser:** Writing – review & editing, Resources. **Clara T. Schoeder:** Writing – review & editing, Resources. **Karsten Mäder:** Resources. **Christian E.H. Schmelzer:** Resources. **Michaela Schulz-Siegmund:** Writing – review & editing, Resources, Conceptualization. **Christian Wölk:** Writing – review & editing, Writing – original draft, Supervision, Resources, Funding acquisition, Conceptualization.

Declaration of competing interest

The authors declare the following financial interests/personal relationships which may be considered as potential competing interests: Christian Woelk reports financial support was provided by German Research Foundation. If there are other authors, they declare that they have no known competing financial interests or personal relationships that could have appeared to influence the work reported in this paper.

Acknowledgements

Financial support for this research was provided by the Deutsche Forschungsgemeinschaft (DFG, German Research Foundation) – project number 396823779 (MK and CW). We express our gratitude to Dr. Jörg Lehmann and Claudia Müller from Fraunhofer IZI for granting us access to the Typhoon™ laser-scanner platform. Additionally, we want to thank Prof. Dr. Thomas Groth, Dr. Adrian Hautmann, Dr. Matheus Regis Belisário Ferrari and Dr. Antonia Sophia Peter for witty, inspiring and helpful conversations. Particular appreciation goes to Felix Krabbes for proofreading and technical support. Images of the graphical abstract were created with servier medical art under the licence CC BY 4.0 <https://creativecommons.org/licenses/by/4.0/>.

Appendix A. Supplementary data

Supplementary material related to this article can be found online at <https://doi.org/10.1016/j.ijpharm.2025.125330>.

Data availability

Data will be made available on request.

References

- Alkhoury, H., Hautmann, A., Erdmann, F., Zhou, G., Stojanović, S., Najman, S., Groth, T., 2020. Study on the potential mechanism of anti-inflammatory activity of covalently immobilized hyaluronan and heparin. *J. Biomed. Mater. Res. - Part A* 108 (5), 1099–1111. <http://dx.doi.org/10.1002/jbm.a.36885>.
- Alkhoury, H., Hautmann, A., Fuhrmann, B., Syrowatka, F., Erdmann, F., Zhou, G., Stojanović, S., Najman, S., Groth, T., 2020. Studies on the mechanisms of anti-inflammatory activity of heparin-and hyaluronan-containing multilayer coatings—targeting NF- κ B signalling pathway. *Int. J. Mol. Sci.* 21 (10), <http://dx.doi.org/10.3390/ijms21103724>.
- Altman, R., Bedi, A., Manjoo, A., Niazi, F., Shaw, P., Mease, P., 2019. Anti-Inflammatory Effects of Intra-Articular Hyaluronic Acid: A Systematic Review. *Cartilage*. vol. 10, (1), SAGE Publications Inc., pp. 43–52. <http://dx.doi.org/10.1177/1947603517749919>.
- Anon, 2023a. EUROPEAN PHARMACOPOEIA 11.0 Chitosan hydrochloride. *Tech. rep.*
- Anon, 2023b. EUROPEAN PHARMACOPOEIA 11.0 Sodium hyaluronate. *Tech. rep.*
- Berger, A.G., Deiss-Yehiely, E., Vo, C., McCoy, M.G., Almofty, S., Feinberg, M.W., Hammond, P.T., 2023. Electrostatically assembled wound dressings deliver pro-angiogenic anti-miRs preferentially to endothelial cells. *Biomaterials* 300, 122188. <http://dx.doi.org/10.1016/j.biomaterials.2023.122188>, URL <https://linkinghub.elsevier.com/retrieve/pii/S0142961223001965>.
- Bernkop-Schnürch, A., Dünnhaupt, S., 2012. Chitosan-based drug delivery systems. In: *European Journal of Pharmaceutics and Biopharmaceutics*. vol. 81, (3), pp. 463–469. <http://dx.doi.org/10.1016/j.ejpb.2012.04.007>.
- Boateng, J., Catanzano, O., 2015. Advanced Therapeutic Dressings for Effective Wound Healing—A Review. *J. Pharm. Sci.* 104 (11), 3653–3680. <http://dx.doi.org/10.1002/jps.24610>.
- Borges, J., Mano, J.F., 2014. Molecular Interactions Driving the Layer-by-Layer Assembly of Multilayers. *Chem. Rev.* 114 (18), 8883–8942. <http://dx.doi.org/10.1021/cr400531v>, URL <https://pubs.acs.org/doi/10.1021/cr400531v>.

- Cantini, M., Donnelly, H., Dalby, M.J., Salmeron-Sanchez, M., 2020. The Plot Thickens: The Emerging Role of Matrix Viscosity in Cell Mechanotransduction. *Adv. Heal. Mater.* 9 (8), <http://dx.doi.org/10.1002/adhm.201901259>.
- Cardoso, M.J., Caridade, S.G., Costa, R.R., Mano, J.F., 2016. Enzymatic Degradation of Polysaccharide-Based Layer-by-Layer Structures. *Biomacromolecules* 17 (4), 1347–1357. <http://dx.doi.org/10.1021/acs.biomac.5b01742>.
- Castleberry, S.A., Almqvist, B.D., Li, W., Reis, T., Chow, J., Mayner, S., Hammond, P.T., 2016. Self-Assembled Wound Dressings MMP-9 and Improve Diabetic Wound Healing in Vivo. *Adv. Mater.* 28 (9), 1809–1817. <http://dx.doi.org/10.1002/adma.201503565>.
- Chou, J.J., Berger, A.G., Jalili-Firoozinezhad, S., Hammond, P.T., 2021. A design approach for layer-by-layer surface-mediated siRNA delivery. *Acta Biomater.* 135, 331–341. <http://dx.doi.org/10.1016/j.actbio.2021.08.042>, URL <https://linkinghub.elsevier.com/retrieve/pii/S1742706121005754>.
- Cipitria, A., Salmeron-Sanchez, M., 2017. Mechanotransduction and Growth Factor Signaling to Engineer Cellular Microenvironments. *Adv. Heal. Mater.* 6 (15), <http://dx.doi.org/10.1002/adhm.201700052>.
- Cunha, M., de Freitas, V., Borges, J., Mano, J.F., Rodrigues, J.M., Cruz, L., 2024. Acidochromic Free-Standing Multilayered Chitosan-Pyranoflavylum/Alginate Membranes toward Food Smart Packaging Applications. *ACS Appl. Polym. Mater.* 6 (11), 6820–6830. <http://dx.doi.org/10.1021/acscamp.4c01085>.
- Demuth, P.C., Min, Y., Huang, B., Kramer, J.A., Miller, A.D., Barouch, D.H., Hammond, P.T., Irvine, D.J., 2013. Polymer multilayer tattooing for enhanced DNA vaccination. *Nat. Mater.* 12 (4), 367–376. <http://dx.doi.org/10.1038/nmat3550>.
- Dimitrova, M., Arntz, Y., Lavalle, P., Meyer, F., Wolf, M., Schuster, C., Haikel, Y., Voegel, J.C., Ogier, J., 2007. Adenoviral gene delivery from multilayered polyelectrolyte architectures. *Adv. Funct. Mater.* 17 (2), 233–245. <http://dx.doi.org/10.1002/adfm.200600155>.
- Facchi, S.P., Souza, P.R., de Almeida, D.A., Madruga, L.Y., Rosseto, P., de Carvalho Nunes, W.M., Kipper, M.J., Martins, A.F., Cardozo-Filho, L., 2023. Surface coatings based on chitosan and tannins applied in the in vivo prevention of corn strobil disease. *Chem. Eng. J.* 477, <http://dx.doi.org/10.1016/j.cej.2023.147003>.
- Flessner, R.M., Jewell, C.M., Anderson, D.G., Lynn, D.M., 2011. Degradable polyelectrolyte multilayers that promote the release of siRNA. *Langmuir* 27 (12), 7868–7876. <http://dx.doi.org/10.1021/la200815t>.
- Fus-Kujawa, A., Prus, P., Bajdak-Rusinek, K., Teper, P., Gawron, K., Kowalczyk, A., Sieron, A.L., 2021. An Overview of Methods and Tools for Transfection of Eukaryotic Cells in vitro. *Front. Bioeng. Biotechnol.* 9, <http://dx.doi.org/10.3389/fbioe.2021.701031>, URL <https://www.frontiersin.org/articles/10.3389/fbioe.2021.701031/full>.
- Hautmann, A., Hedtke, T., Sisilema-Muñoz, S., Martins-Schalinski, J., Schmelzer, C.E., Groth, T., 2024. Design of a composite wound dressing: Combining an electrospun fleece with a free-standing multilayer film. *Next Mater.* 2, 100060. <http://dx.doi.org/10.1016/j.nxmater.2023.100060>.
- Hautmann, A., Kedilaya, D., Stojanović, S., Radenković, M., Marx, C.K., Najman, S., Pietzsch, M., Mano, J.F., Groth, T., 2022. Free-standing multilayer films as growth factor reservoirs for future wound dressing applications. *Biomater. Adv.* 142, <http://dx.doi.org/10.1016/j.bioadv.2022.213166>.
- Hernández-Montelongo, J., Nascimento, V.F., Hernández-Montelongo, R., Beppu, M.M., Cotta, M.A., 2020. Fractal analysis of the formation process and morphologies of hyaluronan/chitosan nanofilms in layer-by-layer assembly. *Polymer* 191, <http://dx.doi.org/10.1016/j.polymer.2020.122283>.
- Holmes, C., Daoud, J., Bagnaninchi, P.O., Tabrizian, M., 2014. Polyelectrolyte Multilayer Coating of 3D Scaffolds Enhances Tissue Growth and Gene Delivery: Non-Invasive and Label-Free Assessment. *Adv. Heal. Mater.* 3 (4), 572–580. <http://dx.doi.org/10.1002/adhm.201300301>.
- Holmes, C.A., Tabrizian, M., 2013. Substrate-mediated gene delivery from glycol-chitosan/hyaluronic acid polyelectrolyte multilayer films. *ACS Appl. Mater. Interfaces* 5 (3), 524–531. <http://dx.doi.org/10.1021/am303029k>.
- Hossfeld, S., Nolte, A., Hartmann, H., Recke, M., Schaller, M., Walker, T., Kjems, J., Schlosshauer, B., Stoll, D., Wendel, H.P., Krastev, R., 2013. Bioactive coronary stent coating based on layer-by-layer technology for siRNA release. *Acta Biomater.* 9 (5), 6741–6752. <http://dx.doi.org/10.1016/j.actbio.2013.01.013>.
- Husteden, C., Brito Barrera, Y.A., Tegtmeyer, S., Borges, J., Giselbrecht, J., Menzel, M., Langner, A., Mano, J.F., Schmelzer, C.E., Wölk, C., Groth, T., 2023. Lipoplex-Functionalized Thin-Film Surface Coating Based on Extracellular Matrix Components as Local Gene Delivery System to Control Osteogenic Stem Cell Differentiation. *Adv. Heal. Mater.* 12 (5), <http://dx.doi.org/10.1002/adhm.202201978>.
- Husteden, C., Doberenz, F., Goergen, N., Pinnapireddy, S.R., Janich, C., Langner, A., Syrowatka, F., Repanas, A., Erdmann, F., Jedelská, J., Bakowsky, U., Groth, T., Wölk, C., 2020a. Contact-Triggered Lipofection from Multilayer Films Designed as Surfaces for in Situ Transfection Strategies in Tissue Engineering. *ACS Appl. Mater. & Interfaces* 12 (8), 8963–8977. <http://dx.doi.org/10.1021/acscami.9b18968>, URL <http://www.ncbi.nlm.nih.gov/pubmed/32003972>.
- Husteden, C., Doberenz, F., Goergen, N., Pinnapireddy, S.R., Janich, C., Langner, A., Syrowatka, F., Repanas, A., Erdmann, F., Jedelská, J., Bakowsky, U., Groth, T., Wölk, C., 2020b. Contact-Triggered Lipofection from Multilayer Films Designed as Surfaces for in Situ Transfection Strategies in Tissue Engineering. *ACS Appl. Mater. Interfaces* 12 (8), 8963–8977. <http://dx.doi.org/10.1021/acscami.9b18968>.
- Janich, C., Pinnapireddy, S.R., Erdmann, F., Groth, T., Langner, A., Bakowsky, U., Wölk, C., 2017. Fast therapeutic DNA internalization – A high potential transfection system based on a peptide mimicking cationic lipid. *Eur. J. Pharmaceut. Biopharmaceut.* 118, 38–47. <http://dx.doi.org/10.1016/j.ejpb.2016.12.007>.
- Janich, C., Wölk, C., Erdmann, F., Groth, T., Brezesinski, G., Dobner, B., Langner, A., 2015. Composites of malonic acid diamides and phospholipids - Impact of lipoplex stability on transfection efficiency. *J. Control. Release* 220, 295–307. <http://dx.doi.org/10.1016/j.jconrel.2015.10.045>.
- Janich, C., Wölk, C., Taföler, S., Drescher, S., Meister, A., Brezesinski, G., Dobner, B., Langner, A., 2014. Composites of malonic acid diamides and phospholipids - Structural parameters for optimal transfection efficiency in A549 cells. *Eur. J. Lipid Sci. Technol.* 116 (9), 1184–1194. <http://dx.doi.org/10.1002/ejlt.201300405>.
- Knopf-Marques, H., Pravda, M., Wolfova, L., Velebný, V., Schaaf, P., Vrana, N.E., Lavalle, P., 2016. Hyaluronic Acid and Its Derivatives in Coating and Delivery Systems: Applications in Tissue Engineering, Regenerative Medicine and Immunomodulation. In: *Advanced Healthcare Materials*. vol. 5, (22), Wiley-VCH Verlag, pp. 2841–2855. <http://dx.doi.org/10.1002/adhm.201600316>.
- Lin, M., Qi, X., 2023. Advances and Challenges of Stimuli-Responsive Nucleic Acids Delivery System in Gene Therapy. *Pharmaceutics* 15 (5), <http://dx.doi.org/10.3390/pharmaceutics15051450>.
- Linnik, D.S., Tarakanchikova, Y.V., Zyuzin, M.V., Lepik, K.V., Aerts, J.L., Sukhorukov, G., Timin, A.S., 2021. Layer-by-Layer technique as a versatile tool for gene delivery applications. *Expert. Opin. Drug Deliv.* 18 (8), 1047–1066. <http://dx.doi.org/10.1080/17425247.2021.1879790>, URL <https://www.tandfonline.com/doi/full/10.1080/17425247.2021.1879790>.
- Liu, M., Ding, R., Li, Z., Xu, N., Gong, Y., Huang, Y., Jia, J., Du, H., Yu, Y., Luo, G., 2024. Hyaluronidase-Responsive Bactericidal Cryogel for Promoting Healing of Infected Wounds: Inflammatory Attenuation, ROS Scavenging, and Immune Regulation. *Adv. Sci.* 11 (17), <http://dx.doi.org/10.1002/advs.202306602>.
- Liu, L., Song, L.N., Yang, G.L., Zhao, S.F., He, F.M., 2011. Fabrication, characterization, and biological assessment of multilayer DNA coatings on sandblasted-dual acid etched titanium surface. *J. Biomed. Mater. Res. - Part A* 97 A (3), 300–310. <http://dx.doi.org/10.1002/jbm.a.33059>.
- McAtee, C.O., Barycki, J.J., Simpson, M.A., 2014. Chapter One - Emerging Roles for Hyaluronidase in Cancer Metastasis and Therapy. In: Simpson, M.A., Heldin, P. (Eds.), *Hyaluronan Signaling and Turnover*. In: *Advances in Cancer Research*, vol. 123, Academic Press, pp. 1–34. <http://dx.doi.org/10.1016/B978-0-12-800092-2.00001-0>.
- Mendes, B.B., Connot, J., Avital, A., Yao, D., Jiang, X., Zhou, X., Sharf-Pauker, N., Xiao, Y., Adir, O., Liang, H., Shi, J., Schroeder, A., Conde, J., 2022. Nanodelivery of nucleic acids. *Nat. Rev. Methods Prim.* 2 (1), 24. <http://dx.doi.org/10.1038/s43586-022-00104-y>, URL <https://www.nature.com/articles/s43586-022-00104-y>.
- Motulsky, H.J., Brown, R.E., 2006. Detecting outliers when fitting data with nonlinear regression – a new method based on robust nonlinear regression and the false discovery rate. *BMC Bioinformatics* 7 (1), 123. <http://dx.doi.org/10.1186/1471-2105-7-123>.
- Nascimento, V., França, C., Hernández-Montelongo, J., Machado, D., Lancellotti, M., Cotta, M., Landers, R., Beppu, M., 2018. Influence of pH and ionic strength on the antibacterial effect of hyaluronic acid/chitosan films assembled layer-by-layer. *Eur. Polym. J.* 109, 198–205. <http://dx.doi.org/10.1016/j.eurpolymj.2018.09.038>.
- Pahal, S., Boranna, R., Tripathy, A., Goudar, V.S., Veetil, V.T., Kurapati, R., Prashanth, G.R., Vemula, P.K., 2023. Nanoarchitectonics for Free-Standing Polyelectrolyte Multilayers Films: Exploring the Flipped Surfaces. In: *ChemNanoMat*. vol. 9, (2), John Wiley and Sons Inc, <http://dx.doi.org/10.1002/cnma.202200462>.
- Piotrowski-Daspiet, A.S., Kauffman, A.C., Bracaglia, L.G., Saltzman, W.M., 2020. Polymeric vehicles for nucleic acid delivery. In: *Advanced Drug Delivery Reviews*. vol. 156, Elsevier B.V., pp. 119–132. <http://dx.doi.org/10.1016/j.addr.2020.06.014>.
- Ponti, F., Campolungo, M., Melchiori, C., Bono, N., Candiani, G., 2021. Cationic lipids for gene delivery: many players, one goal. *Chem. Phys. Lipids* 235, 105032. <http://dx.doi.org/10.1016/j.chemphyslip.2020.105032>, URL <https://linkinghub.elsevier.com/retrieve/pii/S0009308420301638>.
- Rabea, E.I., Badawy, M.E., Stevens, C.V., Smaghe, G., Steurbaut, W., 2003. Chitosan as antimicrobial agent: Applications and mode of action. *Biomacromolecules*. vol. 4, (6), pp. 1457–1465. <http://dx.doi.org/10.1021/bm034130m>.
- Reinhardt, K.A., Kern, W., 2018. Handbook of Silicon Wafer Cleaning Technology. Elsevier, <http://dx.doi.org/10.1016/C2016-0-01001-X>.
- Rosas, M., Sousa, C.F., Pereira, A., Amaral, A.J., Pesqueira, T., Patrício, S.G., Fateixa, S., Nogueira, H.I., Mano, J.F., Oliveira, A.L., Borges, J., 2024. Silk Sericin/Chitosan Supramolecular Multilayered Thin Films as Sustainable Cyto-compatible Nanobiomaterials. *Biomacromolecules* <http://dx.doi.org/10.1021/acs.biomac.4c01146>.
- Saurer, E.M., Jewell, C.M., Roenneburg, D.A., Bechler, S.L., Torrealba, J.R., Hacker, T.A., Lynn, D.M., 2013. Polyelectrolyte multilayers promote stem-mediated delivery of DNA to vascular tissue. *Biomacromolecules* 14 (5), 1696–1704. <http://dx.doi.org/10.1021/bm4005222>.
- Silva, J.M., Caridade, S.G., Costa, R.R., Alves, N.M., Groth, T., Picart, C., Reis, R.L., Mano, J.F., 2015. PH Responsiveness of Multilayered Films and Membranes Made of Polysaccharides. *Langmuir* 31 (41), 11318–11328. <http://dx.doi.org/10.1021/acs.langmuir.5b02478>.

- Sousa, C.F., Monteiro, L.P., Rodrigues, J.M., Borges, J., Mano, J.F., 2023. Marine-origin polysaccharides-based free-standing multilayered membranes as sustainable nanoreservoirs for controlled drug delivery. *J. Mater. Chem. B* 11 (28), 6671–6684. <http://dx.doi.org/10.1039/d3tb00796k>.
- Su, X., Kim, B.S., Kim, S.R., Hammond, P.T., Irvine, D.J., 2009. Layer-by-layer-assembled multilayer films for transcutaneous drug and vaccine delivery. *ACS Nano* 3 (11), 3719–3729. <http://dx.doi.org/10.1021/nn900928u>.
- Sung, Y., Kim, S., 2019. Recent advances in the development of gene delivery systems. *Biomater. Res.* 23 (1), <http://dx.doi.org/10.1186/s40824-019-0156-z>, URL <https://spj.science.org/doi/10.1186/s40824-019-0156-z>.
- Taketa, T.B., Beppu, M.M., 2014. Layer-by-layer thin films of alginate/chitosan and hyaluronic acid/chitosan with tunable thickness and surface roughness. In: *Materials Science Forum*. 783–786, Trans Tech Publications Ltd, pp. 1226–1231. <http://dx.doi.org/10.4028/www.scientific.net/msf.783-786.1226>.
- Talebian, S., Mendes, B., Connot, J., Farajikhah, S., Dehghani, F., Li, Z., Bitoque, D., Silva, G., Naficy, S., Conde, J., Wallace, G.G., 2023. Biopolymeric Coatings for Local Release of Therapeutics from Biomedical Implants. *Adv. Sci.* 10 (12), <http://dx.doi.org/10.1002/advs.202207603>, URL <https://onlinelibrary.wiley.com/doi/10.1002/advs.202207603>.
- Wang, J., Hu, Y., Han, Y., Fang, Q., Chen, Z., Wang, Y., Zhao, P., Wang, H., Lin, Q., 2023. Non-viral gene coating modified IOL delivering PDGFR- α shRNA interferes with the fibrogenic process to prevent posterior capsular opacification. *Regen. Biomater.* 10, <http://dx.doi.org/10.1093/rb/rbad020>.
- Wenzel, R.N., 1936. Resistance of solid surfaces to wetting by water. *Ind. Eng. Chem.* 28 (8), 988–994, URL <https://pubs.acs.org/sharingguidelines>.
- Wey, K., Schirrmann, R., Diesing, D., Lang, S., Brandau, S., Hansen, S., Epple, M., 2021. Coating of cochlear implant electrodes with bioactive DNA-loaded calcium phosphate nanoparticles for the local transfection of stimulatory proteins. *Biomaterials* 276, <http://dx.doi.org/10.1016/j.biomaterials.2021.121009>.
- Xie, L., Ding, X., Budry, R., Mao, G., 2018. Layer-by-layer DNA films incorporating highly transfecting bioreducible poly(Amido amine) and polyethylenimine for sequential gene delivery. *Int. J. Nanomedicine* 13, 4943–4959. <http://dx.doi.org/10.2147/IJN.S162353>.
- Yamauchi, F., Koyamatsu, Y., Kato, K., Iwata, H., 2006. Layer-by-layer assembly of cationic lipid and plasmid DNA onto gold surface for stent-assisted gene transfer. *Biomaterials* 27 (18), 3497–3504. <http://dx.doi.org/10.1016/j.biomaterials.2006.02.004>.
- Yang, R., Chen, F., Guo, J., Zhou, D., Luan, S., 2020. Recent advances in polymeric biomaterials-based gene delivery for cartilage repair. *Bioact. Mater.* 5 (4), 990–1003. <http://dx.doi.org/10.1016/j.bioactmat.2020.06.004>.
- Zhang, Y., Ma, W., Zhan, Y., Mao, C., Shao, X., Xie, X., Wei, X., Lin, Y., 2018. Nucleic acids and analogs for bone regeneration. *Bone Res.* 6 (1), 37. <http://dx.doi.org/10.1038/s41413-018-0042-7>.
- Zou, Y., Xie, L., Carroll, S., Muniz, M., Gibson, H., Wei, W.Z., Liu, H., Mao, G., 2014. Layer-by-layer films with bioreducible and nonbioreducible polycations for sequential DNA release. *Biomacromolecules* 15 (11), 3965–3975. <http://dx.doi.org/10.1021/bm5010433>.